Delayed discrete memristive ring neural network and application in pseudorandom number generator

Gang Yang, Chunhua Wang, Yichuang Sun *Senior Member, IEEE*, Quanli Deng

***Abstract*—Synaptic delay effects play a crucial role in biological neural networks, influencing the dynamical behaviors of neural networks. However, the dynamical characteristics of neural networks based on discrete memristors with synaptic delay effects have not yet been thoroughly investigated. This paper presents a novel discrete memristor model with delay effects and incorporates it as an autapse into a ring Hopfield neural network to simulate biological synapse delay properties, constructing a delayed discrete memristive ring neural network (DDMRNN). The system's dynamical behavior becomes significantly more complex as the delay length increases. Through modulation of the synapse weight w_{11}, the system exhibits rich dynamical evolution properties, including diversified attractors, transient chaos, and synapse weight-dependent offset-boosting. Additionally, coexisting behaviors of homogeneous and heterogeneous chaotic attractors are revealed under varying initial conditions. FPGA-based hardware experiments validate the implementability of the DDMRNN circuit. Furthermore, the application of DDMRNN to pseudorandom number generation demonstrates that the produced sequences successfully pass stringent statistical randomness tests, confirming the system's potential applicability in information security domains.**

***Index Terms*—Delay effect, discrete memristor, neural network, complex dynamics, pseudorandom number generator.**

I. Introduction

In the information transmission process of biological neural systems, the delay effects exhibited by synaptic activity represent a nonlinear phenomenon of significant dynamical importance [1], [2]. From a biophysical mechanism perspective, synaptic delay originates from nonlinear physiological processes, such as the stochasticity of neurotransmitter release, the spatiotemporal dynamics of the diffusion process, and the threshold characteristics of the receptor activation [3], [4]. Research demonstrates that synaptic delay, by modulating the phase-coupling relationships of neural signals, not only facilitates the formation of spike-timing-dependent plasticity (STDP), a crucial nonlinear learning mechanism [5], but its delayed feedback feature can also induce diverse nonlinear dynamical behaviors in networks, including multistable switching, chaotic oscillations, and synchronized clusters [6]–[8]. These nonlinear phenomena provide neuromorphic computing with enhanced functionalities such as dynamic memory storage and brain-like information processing. Therefore, in-depth exploration of the nonlinear dynamical mechanisms underlying synaptic delays and their biomimetic implementation holds significant theoretical and practical value for developing biologically plausible artificial intelligence systems.

Memristors, as a new type of electronic device with memory effects and nonlinear characteristics, have attracted extensive attention within the fields of electronic engineering and computer science. The unique resistive memory property of this device demonstrates significant application potential across various domains, with notable advancements particularly achieved in-memory computing [9], chaotic systems [10], [11], and non-volatile memory [12]. Additionally, the synapse-like properties of memristors provide efficient and feasible solutions for biomimetic circuit design [13], [14] and artificial neural networks [15], [16], greatly advancing the development of neuromorphic computing. Discrete memristors offer unique advantages in constructing complex dynamical systems due to their memristive properties and discrete nature. Even when employing simple chaotic maps or neural network structures, they can generate rich nonlinear dynamical behaviors [17], [18]. Wang et al [19] designed a five-dimensional discrete memristive hyperchaotic map by coupling four discrete memristors in a hybrid parallel-cascaded configuration with the sine map. This system exhibits extreme multistability and high spectral entropy complexity. Luo et al [20] proposed three discrete memristor models and constructed three hyperchaotic maps with high Lyapunov exponents by introducing the nonlinear oscillatory terms into the memristors. Lai et al [21] introduced a unified framework for constructing four-dimensional hyperchaotic maps based on the memristor, unveiling numerous coexisting attractors, controllable amplitude modulation, and parameter-driven attractor offset-boosting. Although various novel discrete memristors and their corresponding chaotic maps have been successively proposed and extensively studied. However, discrete memristors with delay effects remain insufficiently investigated.

Neural networks with complex nonlinear dynamics hold profound scientific significance for revealing the intrinsic dynamical principles underlying brain cognitive functions [22]. As a classical type of recurrent neural network model, Hopfield neural networks (HNNs) can exhibit rich dynamical behaviors due to their distinctive fully-connected recurrent architecture, associative memory properties, asynchronous update mechanisms, and nonlinear activation functions [23]–[25]. In recent years, investigations into the dynamical characteristics of HNNs have attracted widespread attention [26]–[28]. Zhang et al. [29] constructed a no-equilibrium memristive

Manuscript received Month xx, 2xxx; revised Month xx, xxxx; accepted Month x, xxxx. This work was supported in part by the National Natural Science Foundation of China under Grants 62271197 and 62571183, and in part by the Guangdong Basic and Applied Basic Research Foundation under Grant 2024A1515011910.

Gang Yang, Chunhua Wang, and Quanli Deng are with the College of Information Science and Engineering, Hunan University, Changsha, 410082, China (Corresponding author: Chunhua Wang, e-mail: wch1227164@hnu.edu.cn).

Chunhua Wang is also with the Greater Bay Area Institute for Innovation, Hunan University, Guangzhou, 511300, China.

Yichuang Sun is with the School of Engineering and Computer Science, University of Hertfordshire, Hatfield AL10 9AB, U.K.

ring neural network, where one memristor emulates neural synapses and another serves as an external electronic radiation source. This system exhibits complex dynamical behaviors, including attractor growing, coexisting multistability, and diverse firing patterns. Zhang et al. [30] further investigated the ring-structured HNN by integrating two memristors into the neural network. An undirected ring neural network with multi-scroll hidden attractors, diverse coexisting attractors, and hidden multistability is proposed. The construction of traditional continuous HNNs typically requires at least three neurons to achieve complex dynamical behaviors. However, Bao et al [31] adopted a simple neural network structure containing only two non-self-connecting neurons in the discrete domain, successfully designing a discrete two-neuron HNN featuring polyhedral hyperchaotic attractors and multiple coexisting attractors. Bao et al [32] subsequently developed a novel discrete memristive HNN by incorporating a discrete adaptive memristor to emulate synaptic connections between neurons.

Currently, enhancing the complexity of chaotic maps primarily relies on introducing nonlinear terms and discrete memristors. Notably, the delayed feedback mechanism offers a novel research approach for strengthening chaotic dynamical characteristics. Liu et al. [33] significantly enhanced the complexity, ergodicity, dimensionality, and chaotic range of chaotic maps by combining delayed feedback with the modulus operation method, effectively addressing the fragility and degradation issues present in traditional chaotic systems. Deng et al. [34] further integrated the delayed feedback mechanism with the memristor-based chaotic map, proposing a universal delayed differential feedback memristor map. The introduction of the time delay dramatically improves the dynamic behavior of the system. Inspired by the time-delay effects in biological neural systems, Deng et al. [35] further extended this mechanism to the field of neuron modeling, constructing a discrete memristor-based delayed feedback Rulkov neuron, which exhibits richer complex dynamical behaviors. It should be noted that compared to continuous systems with time delays, discrete systems with time delays possess a distinct advantage: the inherent discrete nature of discrete systems aligns highly with time delay mechanisms. Their state space can be expanded arbitrarily while still being effectively confined within finite dimensions. In contrast, time-delay-based continuous systems result in an infinite increase in system dimensions, and their state space becomes correspondingly infinite-dimensional [36]. However, the neurodynamics of neural networks with delayed discrete memristors remains unreported and requires further in-depth investigation.

Inspired by the aforementioned studies, this paper proposes a discrete memristor model with delay effects to simulate the synaptic delay in neural systems. By embedding the delayed discrete memristor into a three-neuron ring HNN, we constructed a novel DDMRNN. Theoretical analysis and numerical simulations demonstrate that the system's dynamical complexity prominently increases with increasing delay length. The study reveals diverse nonlinear dynamical behaviors, including dynamical evolution, transient chaos, synapse weight-dependent offset boosting, and the coexistence of homogeneous and heterogeneous attractors. Furthermore, an FPGA-based hardware implementation of DDMRNN is developed. Advancing the application potential, we designed a DDMRNN-based pseudo-random number generator (PRNG), whose robust randomness is verified through NIST statistical tests and the test suite TestU01.

This paper makes the following innovative contributions:

1) Inspired by the synaptic delay characteristics in biological neural systems, we propose a discrete memristor model with delay effects to simulate the autaptic connections in the ring HNN, thereby constructing a novel DDMRNN. Mathematical theoretical analysis demonstrates that the system possesses countless unstable fixed points.

2) Through dynamical analysis, we find that increasing the delay length significantly enhances the dynamical complexity of DDMRNN. The system exhibits rich nonlinear behaviors, including complex dynamical evolution, transient chaos, synapse weight-dependent offset-boosting, and coexistence of homogeneous and heterogeneous attractors.

3) The DDMRNN circuit is implemented on an FPGA hardware platform, and experimental results confirm the feasibility and correctness of its hardware realization. Moreover, the PRNG designed based on DDMRNN produced random sequences that passed the full suite of NIST statistical tests and the test suite TestU01, demonstrating the system's capability to generate high-quality pseudo-random numbers.

The remainder of this paper is organized as follows. Section II elaborates on the mathematical models of the delayed discrete memristor and DDMRNN, and conducts a theoretical analysis of the system's fixed points and stability. Section III investigates the impact of delay length on the dynamic characteristics of DDMRNN and uncovers various complex nonlinear behaviors. Section IV implements the hardware circuit of DDMRNN on an FPGA platform and constructs a PRNG based on DDMRNN, evaluating its randomness performance through standard tests. Section V concludes the paper and provides future research perspectives.

II. CONSTRUCTION OF DDMRNN

In this section, the mathematical models of the delayed discrete memristor and DDMRNN are described, and the fixed point and stability of the system are analyzed.

A. Delayed Discrete Memristor Model

To explore synapse delay effects of neural networks, delayed feedback control is introduced into a memristor. Based on the Euler difference method, a delayed discrete memristor is defined as:

$$\begin{cases} i(n) = W(\varphi(n))v(n) = \sin(\varphi(n))v(n) \\ \varphi(n+1) = \varphi_1(n) + \alpha\tanh(v(n)) + \beta\sin(v(n)) \\ \varphi_1(n+1) = \varphi_2(n) \\ \cdots \\ \varphi_{D-1}(n+1) = \varphi_D(n) \\ \varphi_D(n+1) = \varphi(n) \end{cases} \tag{1}$$

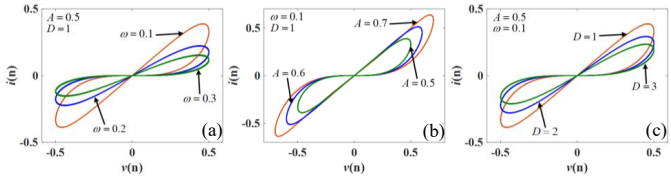

Fig. 1: Fingerprint features of the delayed discrete memristor. (a) Frequency-related pinched hysteresis loops with $A = 0.5$ and $D = 1$. (b) Amplitude-related pinched hysteresis loops with $\omega = 0.1$ and $D = 1$. (c) Delay-related pinched hysteresis loops with $A = 0.5$ and $\omega = 0.1$.

where $i(n)$, $v(n)$, and $\varphi(n)$ represent the n-th iterative values of current, voltage, and flux, respectively. $W(\varphi(n)) = \sin(\varphi(n))$ denotes the memductance. α and β are the discrete memristor parameters. And D signifies the delay length.

To verify the essential characteristics of this delayed discrete memristor, the memristor parameters are set as $\alpha = 0.1$, $\beta = 0.1$, and a discrete input voltage source $v(n) = A\sin(\omega n)$ is employed. When the amplitude $A = 0.5$ and delay length $D = 1$, the hysteresis loops with frequencies $\omega = 0.3$, 0.2, and 0.1 are shown in Fig. 1(a). When the frequency $\omega = 0.1$ and delay length $D = 1$, the hysteresis loops under different amplitudes $A = 0.7$, 0.6, and 0.5 are presented in Fig. 1(b). By fixing the amplitude $A = 0.5$ and frequency $\omega = 0.1$, the hysteresis loops affected by different delay lengths $D = 1$, 2, and 3 are illustrated in Fig. 1(c). The simulation results in Fig. 1 exhibit that as the frequency increases, the lobe area of the hysteresis loop decreases, whereas increasing the amplitude leads to an expansion of the lobe area. Furthermore, the lobe area shrinks with increasing delay length. These fingerprint characteristics confirm the memristor properties of this delayed discrete memristor.

B. DDMRNN Model

In the discrete domain, the dynamics of memristor-based HNNs with ring-connected structures have rarely been investigated. Based on a three-neuron HNN, we introduce the proposed delayed discrete memristor as a self-synapse to construct a DDMRNN, whose structure is illustrated in Fig. 2. Consequently, the mathematical formulation of the DDMRNN can be expressed as:

$$\begin{cases} x(n+1) = 0.8x(n) + w_{11}\tanh(x(n)) + 2\tanh(y(n)) \\ y(n+1) = y(n) - 5\tanh(y(n)) - 5\tanh(z(n)) \\ z(n+1) = 0.1z(n) + \tanh(x(n)) + k\tanh(z(n))\times \\ \qquad \sin(w(n)) \\ w(n+1) = w_1(n) + 0.1\tanh(\tanh(z(n))) \\ \qquad +0.2\sin(\tanh(z(n))) \\ w_1(n+1) = w_2(n) \\ \cdots \\ w_{D-1}(n+1) = w_D(n) \\ w_D(n+1) = w(n) \end{cases} \tag{2}$$

where $x(n)$, $y(n)$, and $z(n)$ represent the membrane potentials of the three HNN neurons, respectively. w_{11} denotes the connection weight. k stands for the coupling strength. $w(n)$ is the state variable of the delayed discrete memristor, and D represents the delay length.

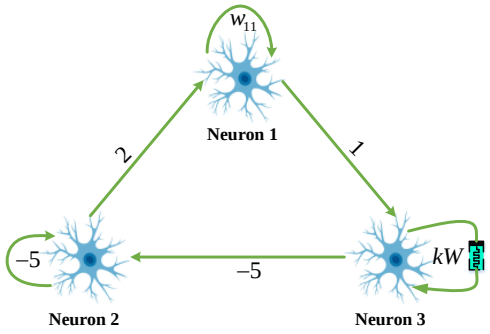

Fig. 2: Connection structure diagram of DDMRNN based on a three-neuron HNN.

C. Fixed Point and Stability

The stability of DDMRNN can be assessed by its fixed point. Assuming the fixed point as $P(X, Y, Z, W, \cdots, W_D)$, the following equation can be derived to calculate the corresponding fixed point P:

$$\begin{cases} X = 0.8X + w_{11}\tanh(X) + 2\tanh(Y) \\ Y = Y - 5\tanh(Y) - 5\tanh(Z) \\ Z = 0.1Z + \tanh(X) + k\tanh(Z)\sin(W) \\ W = W_1 + 0.1\tanh(\tanh(Z)) + 0.2\sin(\tanh(Z)) \\ W_1 = W_2 \\ \cdots \\ W_{D-1} = W_D \\ W_D = W \end{cases} \tag{3}$$

From Eq. (3), we obtain $W = W_1 = W_2 = \cdots = W_D$, which allows the fourth equation to be simplified to $0.1\tanh(\tanh(Z)) + 0.2\sin(\tanh(Z)) = 0$. It can be deduced that $Z = 0$, which subsequently yields $X = Y = 0$. Thus, the fixed point P can be represented as $(0, 0, 0, \eta, \eta, \cdots, \eta)$ (η is an arbitrary value), and DDMRNN has an infinite number of fixed points.

Set the eigenvalues of the Jacobian matrix at fixed point P to $(\lambda_1, \lambda_2, \cdots, \lambda_{D+4})$. The stability of the fixed point is determined as follows: If any absolute eigenvalue $|\lambda_i| > 1$ $(i = 1, 2, \cdots, D+4)$, the fixed point is unstable; If all absolute eigenvalues $|\lambda_i| < 1$, then the fixed point is stable. By fixing the parameters $w_{11} = 1$, $k = 1$, and delay length $D = 3$, the eigenvalues can be computed from the following Jacobian matrix expression:

$$J_P = \begin{bmatrix} f'_1(X) & f'_1(Y) & \cdots & f'_1(W_3) \\ f'_2(X) & f'_2(Y) & \cdots & f'_2(W_3) \\ \vdots & \vdots & \ddots & \vdots \\ f'_7(X) & f'_7(Y) & \cdots & f'_7(W_3) \end{bmatrix}_{7\times 7} \tag{4}$$

where $f'_i(X), f'_i(Y), \cdots, f'_i(W_3)$ $(i = 1, 2, \cdots, 7)$ are the first-order partial derivatives of Eq. (3), for instance $f'_1(X) =$

TABLE I: PARAMETERS, FIXED POINTS, EIGENVALUES, AND STABILITY OF DDMRNN

Parameters	Fixed Points	Eigenvalues	Stability
$w_{11}=1$, $k=1$, $D=3$	$(0,0,0,0,0,0,0)$	$-4.3635, 1.1317 \pm 1.0844\text{i}, \pm 1, \pm\text{i}$	Unstable
	$(0,0,0,0.5,0.5,0.5,0.5)$	$-4.3320, 1.3557 \pm 1.1972\text{i}, \pm 1, \pm\text{i}$	Unstable
	$(0,0,0,1,1,1,1)$	$-4.3115, 1.5265 \pm 1.2496\text{i}, \pm 1, \pm\text{i}$	Unstable
	$(0,0,0,1.5,1.5,1.5,1.5)$	$-4.3034, 1.6004 \pm 1.2644\text{i}, \pm 1, \pm\text{i}$	Unstable
	$(0,0,0,2,2,2,2)$	$-4.3079, 1.5586 \pm 1.2566\text{i}, \pm 1, \pm\text{i}$	Unstable
	$(0,0,0,2.5,2.5,2.5,2.5)$	$-4.3250, 1.4117 \pm 1.2173\text{i}, \pm 1, \pm\text{i}$	Unstable
	$(0,0,0,3,3,3,3)$	$-4.3537, 1.1974 \pm 1.1233\text{i}, \pm 1, \pm\text{i}$	Unstable
	$(0,0,0,3.5,3.5,3.5,3.5)$	$-4.3903, 0.9697 \pm 0.9623\text{i}, \pm 1, \pm\text{i}$	Unstable
	$\vdots$	$\vdots$	$\vdots$

$0.8 + \text{sech}^2(X)$. Table I summarizes the fixed points of the DDMRNN, the corresponding eigenvalues of the Jacobian matrix, and their stability. It can be observed that these fixed points are unstable, which can drive the formation of chaotic attractors.

III. DYNAMIC ANALYSIS OF DDMRNN

This section investigates the influence of the discrete memristor's delay length on the dynamic characteristics of DDMRNN, and conducts an in-depth analysis of the dynamical behaviors dependent on synapse weight w_{11} and initial conditions. Moreover, the chaotic sequence generated by the system is tested and compared.

A. Dynamics Influenced by Delayed Memristor

The numerical results in Fig. 1(c) demonstrate that the characteristic curves of the delayed discrete memristor vary with increasing delay length. Therefore, this study investigates the dynamical behaviors of DDMRNN when the memristor's delay length is modulated.

Select the synapse weight $w_{11} = 1$, initial values $(x_0, y_0, z_0) = (0.1, 0.1, 0.1)$, and set the initial values of the delayed discrete memristor to 0. When the delay length D takes values of 0, 1, 2, and 3, the Lyapunov exponent (LE) spectra and bifurcation diagrams for the variation of the coupling strength k in the range of [-5,5] are shown in Fig. 3. The simulation results in Fig. 3(a) present that in the absence of delay effect, the system has only one positive LE in the interval $k \in [-5, 5]$, along with multiple periodic windows. With the stimulus of delay length $D = 1$, we can see from Fig. 3(b) that some of the original periodic windows disappear and transition into chaotic states, so the whole chaotic range of the system becomes wider. When the delay length is increased to 2, the LE spectra and bifurcation diagram in Fig. 3(c) reveal that the system no longer exhibits periodic windows within the range $k \in [-5, 5]$. Moreover, LE_2 also becomes positive, indicating a transition from chaotic to hyperchaotic behavior. Further increasing the delay length D, it can be found by comparing Figs. 3(c) and (d) that under the influence of extended delay length, the system possesses three positive LEs, and the bifurcation diagram demonstrates denser distribution of point, reflecting more complex dynamical properties. Meanwhile, an increase in the number of positive LE in a chaotic system indicates the presence of exponential divergence in multiple independent directions within the phase space, which corresponds to a higher fractal dimension. This implies more intricate dynamical behavior in the system's evolution.

From the above analysis, it can be inferred that as the delay length increases, the dynamical behavior of DDMRNN transitions from chaotic to hyperchaotic states, accompanied by an expansion of the chaotic range and an increase in complexity of its chaotic characteristics.

To thoroughly analyze the dynamic effects of the delay length D on the system, the Kaplan-Yorke dimension is adopted as an evaluation metric. The Kaplan-Yorke dimension is a method for calculating the fractal dimension of a strange attractor based on Lyapunov exponents, which correlates the dynamic characteristics of a system with its fractal structure. It serves as a numerical measure of the complexity of a dynamical system. Under the condition that the coupling strength k is set to 1, other parameters and initial values remain unchanged, the Kaplan-Yorke dimension of the system varies with the delay length D as shown in Fig. 4. It can be observed that as D increases, the Kaplan-Yorke dimension exhibits a linear upward trend, indicating an enhancement in the dynamic complexity of the system. Therefore, increasing the delay length D can effectively enhance the dynamic complexity of the system.

B. Dynamical Evolution Behavior

To elucidate the dynamical evolution behavior of DDMRNN, the coupling strength and delay length are fixed at $(k, D) = (1, 3)$, and the initial conditions are set as $(0.1, 0.1, 0.1, 0, 0, 0, 0)$. Fig. 5 depicts the phase portraits in the x-y plane for different values of the synapse weight w_{11}. As shown in Fig. 5, the topological structure of the attractor changes with the variation of the synapse weight

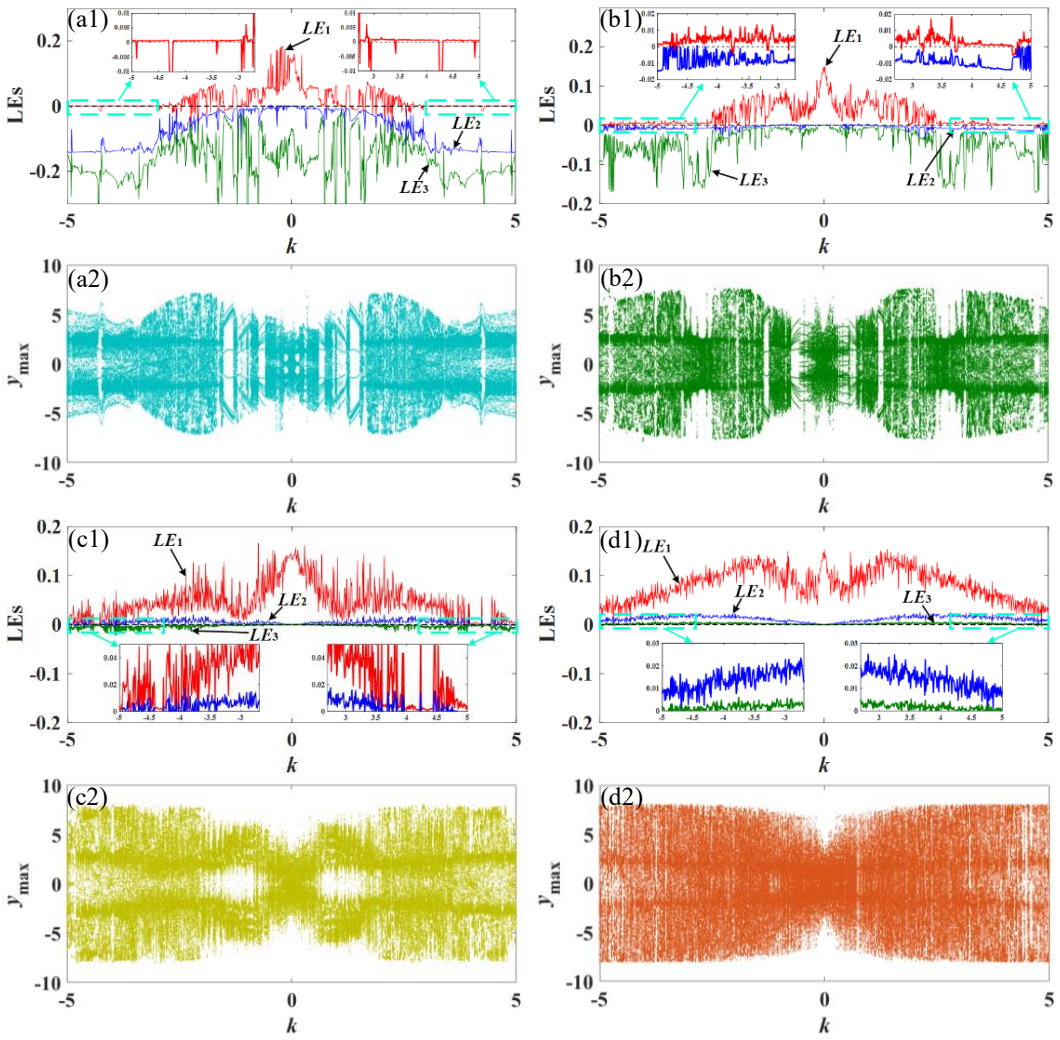

Fig. 3: Dynamical behaviors of DDMRNN under varying delay lengths for $w_{11} = 1$ and $k \in [-5, 5]$. (a) LE spectra and bifurcation diagram with $D = 0$. (b) LE spectra and bifurcation diagram with $D = 1$. (c) LE spectra and bifurcation diagram with $D = 2$. (d) LE spectra and bifurcation diagram with $D = 3$.

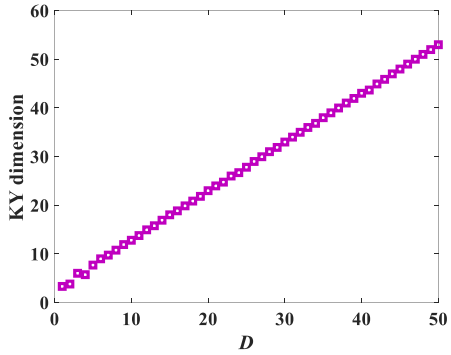

Fig. 4: Analysis result on the correlation between delay length and D_{KY}.

w_{11}, indicating the evolution of the system's dynamics. To further study this behavior, the corresponding LE spectra and bifurcation diagram are plotted in Fig. 6 with w_{11} as the variable. Clearly, the system exhibits more than one positive LE within the internal $w_{11} \in [-10, -1.1]$, maintaining hyperchaotic behavior. When $w_{11} \in [-1.11, 1.1]$, although the system still has a positive LE, the bifurcation diagram displays periodic point. This means that a transition from chaotic to periodic dynamics, and the system undergoes transient chaos, as shown in Fig. 5(f). The time series of the x-sequence for this state is shown in Fig. 7, where a transition from chaotic to periodic behavior can be observed. Next, the system transitions from hyperchaotic behavior in the range of $w_{11} \in [1.11, 2.37]$ to chaotic behavior in the range of $w_{11} \in [2.37, 10]$ This continuously evolving dynamical behavior leads to the generation of various strange attractors by the DDMRNN.

Notably, within the interval [2.38,10] in Fig. 6(b), as w_{11} increases, the dense points continue to shift upward along the x-direction, suggesting the occurrence of an offset-boosting phenomenon in the system. Fig. 8 illustrates the x-y chaotic attractors for $w_{11} = 4$, 6, 8, and 10. The four homogeneous attractors are located at different positions in the x-y plane, further validating the w_{11}-dependent offset-boosting feature.

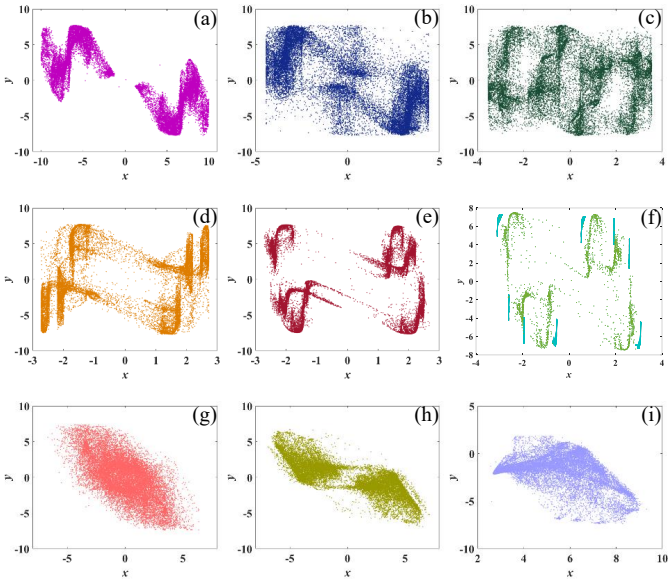

Fig. 5: Phase portraits of the attractors in the x-y plane for different values of w_{11}. (a) $w_{11} = -10$. (b) $w_{11} = -4$. (c) $w_{11} = -3$. (d) $w_{11} = -2$. (e) $w_{11} = -1.3$. (f) $w_{11} = -1$. (g) $w_{11} = 1$. (h) $w_{11} = 2$. (i) $w_{11} = 2.5$.

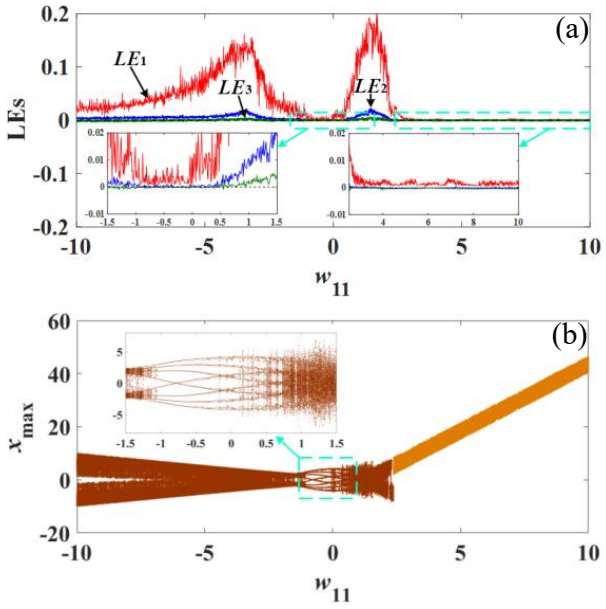

Fig. 6: For $(k, D) = (1, 3)$, the LE spectra and bifurcation diagram with respect to w_{11}. (a) LE spectra. (b) bifurcation diagram.

C. Homogeneous and Heterogeneous Coexisting Attractors

The network parameters and delay length are set to $(w_{11}, k, D) = (4, 1, 3)$, and the initial values are selected as $(x(0), y(0), z(0), w(0), w1(0), w2(0), w3(0)) = (x(0), 0.1, 0.1, 0, 0, 0, 0)$. When the initial values $x(0)$ are -1, 0, and 1, respectively, three chaotic attractors generated by the DDMRNN coexist in the x-y plane, as shown in Fig. 9(a). Homogeneous attractors possess the identical structure, and heterogeneous attractors exhibit different structures. Consequently, the dark purple marked attractor and the light cyan marked attractor constitute a pair of symmetrically homogeneous coexisting attractors about the origin. In contrast, the blue marked attractor coexists heterogeneously with the other two attractors. To explore the coexisting behaviors for other initial values, Fig. 9(b) presents the basin of attraction in the $x(0)$-$y(0)$ plane. The yellow and blue marked regions correspond to the attractors labeled by dark purple and light cyan, respectively. As can be observed, the basin of attraction consists of domains occupied by these two types of homogeneous attractors, and the heterogeneous attractors exhibit an extremely small basin of attraction in the $x(0)$-$y(0)$ plane. To present the results more clearly, its precise location is marked with a bright cyan box in Fig. 9(b), and its detailed range is shown in Fig. 9(c).

Additionally, fixing the synapse weight w_{11} and initial value $x(0)$ to 1 and 0.1, and only varying the initial value $w(0)$, Fig. 10 depicts the z-w chaotic attractors for different $w(0)$ values. The four coexisting chaotic attractors show distinctly different structures, confirming their heterogeneous coexistence. These observations demonstrate that both homogeneous and heterogeneous coexisting attractors in the DDMRNN exhibit diversified initial-dependent coexisting behaviors.

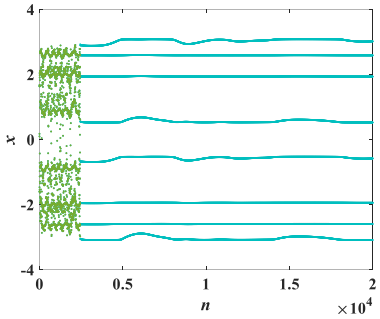

Fig. 7: For $w_{11} = -1$, the x-sequence of the system transitions from chaos to periodicity.

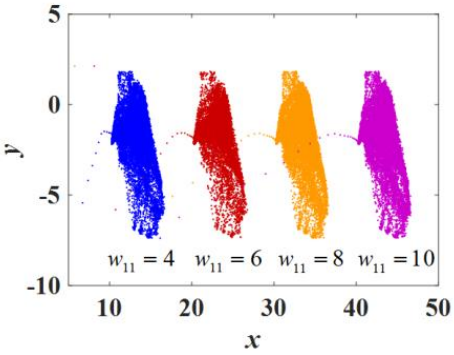

Fig. 8: For $(k, D) = (1, 3)$, offset-boosting homogeneous chaotic attractors for $w_{11} = 4$, 6, 8, and 10.

D. Performance Evaluations

We select several metrics to evaluate the performance of DDMRNN, including approximate entropy (AE), dispersion entropy (DE), increment entropy (IE), phase entropy (PE), and sample entropy (SE). For comparison, we benchmarked

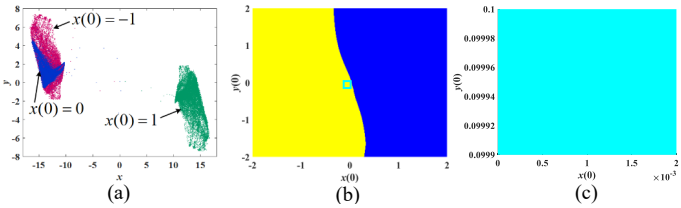

Fig. 9: For $(w_{11}, k, D) = (4, 1, 3)$, the initial coexisting dynamics of DDMRNN. (a) Coexisting homogeneous and heterogeneous attractors with $x(0) = -1$, 0, and 1. (b) Basin of attraction in the $x(0)$-$y(0)$ plane (The region marked by the bright cyan box represents the basin of the heterogeneous attractors, and its specific range is shown in subplot (c)). (c) The basin of attraction corresponding to the heterogeneous attractors in the $x(0)$-$y(0)$ plane.

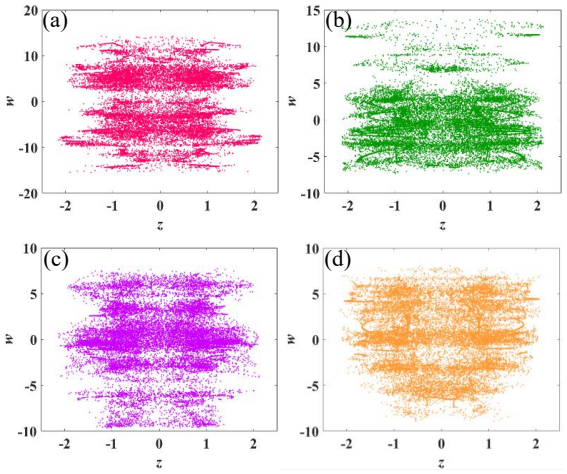

Fig. 10: For $(w_{11}, k, D) = (1, 1, 3)$, Coexisting heterogeneous chaotic attractors with different initial values $w(0)$. (a) $w(0) = -2$. (b) $w(0) = -1$. (c) $w(0) = 0$. (d) $w(0) = 2$.

against existing delayed chaotic maps and high-dimensional chaotic maps. All test sequences are fixed at a length of 10000 points.

Table II presents the parameter configurations, initial value settings, and test results of different chaotic maps. From the experimental results, it can be seen that as the delay length D increases, the entropy values of the chaotic sequences generated by the system generally exhibit an upward trend. Although when $D = 2$, the DE value is slightly higher than the results under the other three delay lengths. Compared with other chaotic maps, when $D = 3$, the chaotic sequences produced by DDMRNN outperform all other chaotic maps across all five metrics, particularly with IE and PE exceeding 4.45 and 0.85, respectively. This performance test reflects DDMRNN's intricate dynamical behavior and randomness, thereby confirming its suitability for chaotic-based applications.

IV. HARDWARE IMPLEMENTATION AND APPLICATION IN PRNG

In this section, DDMRNN is implemented and validated on an FPGA hardware platform. Subsequently, a PRNG based on DDMRNN is established, and the randomness of the generator is evaluated using the NIST SP800-22 test suite.

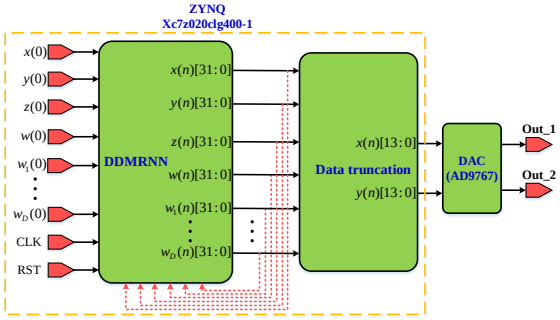

Fig. 11: Hardware system design flow of the FPGA-based DDMRNN.

A. FPGA Hardware Implementation

The circuit design and verification of chaotic systems constitute a critical research component for engineering applications. Currently, digital circuits have emerged as the main technical approach for implementing chaotic maps, owing to their advantages including high-speed computation, stability, parallel processing, and programmability. It is noteworthy that the inherent discretization characteristics of chaotic maps exhibit a high degree of compatibility with the operational mechanisms of digital circuits, endowing them with natural adaptability for design and implementation on digital circuit platforms. In this circuit experiment, we utilize an FPGA hardware platform to implement and validate the hardware design of DDMRNN. The experimental equipment mainly consists of a Xilinx xc7z020clg400-1 development board, a digital-to-analog converter (AD9767), and an oscilloscope.

Fig. 11 illustrates the hardware system design flow of the FPGA-based DDMRNN. In this process, the DDMRNN core computation module adopts a 32-bit fixed-point format to define network parameters and variables, with a data format consisting of 1 sign bit, 6 integer bits, and 25 fractional bits. After completing the iterative computations, the module transfers the operational results to a data truncation module for precision conversion. The data truncation module downsamples the 32-bit intermediate data to 14-bit output signals to meet the bit-width requirements of the subsequent digital-to-analog conversion interface. The processed digital signals are converted into analog signals by the DAC module (AD9767), and are finally collected and visualized by the oscilloscope, displaying phase diagram trajectories that characterize the system's dynamic behavior.

During the design process, the tanh and sin functions are computed using the rotation mode of the CORDIC algorithm. The unified iterative equation of this algorithm is as follows:

$$\begin{cases} U_{i+1} = k_n(U_i - \mu\sigma_i 2^{-i} V_i) \\ V_{i+1} = k_n(V_i + \sigma_i 2^{-i} U_i) \\ W_{i+1} = W_i - \sigma_i \theta_i \end{cases} \tag{5}$$

$$k_n = \prod_{i=0}^{n-1} \sqrt{1 + \mu 2^{-2i}} \tag{6}$$

TABLE II: PERFORMANCE EVALUATION FOR DIFFERENT CHAOTIC MAPS

Chaotic Maps	Parameters	Initial Values	AE	DE	IE	PE	SE
DDMRNN	$(w_{11}, k, D) = (1, 1, 3)$	(0.1,0.1,0.1,0,0,0,0)	2.2357	1.8886	4.4535	0.8714	2.1802
	$(w_{11}, k, D) = (1, 1, 2)$	(0.1,0.1,0.1,0,0,0)	2.0628	2.0288	4.3305	0.8487	2.0036
	$(w_{11}, k, D) = (1, 1, 1)$	(0.1,0.1,0.1,0,0)	1.9974	1.7065	4.1220	0.8331	1.9457
	$(w_{11}, k, D) = (1, 1, 0)$	(0.1,0.1,0.1,0)	1.8961	1.6093	3.5233	0.7236	1.7990
Xu [10]	$(a, b, c, d, e, k_0, k_1, k_2) = (1.2, 0.1, -1.2, 1.72, \pi/6, 0.1, -10, 0.5)$	(0.5,0.5,0.1,0.1)	2.2251	1.6870	3.7178	0.5057	2.1688
Wang [19]	$(a, k_1, k_2, k_3, k_4) = (1.4, 0.6, 1.6, 0.6, 0.9)$	(0.1,0.1,0.1,0.1,0)	2.0241	1.3985	2.8202	0.4417	1.9877
Deng [34]	$k = 1$	(0.1,0.1,0,0,0,0,0)	2.0597	1.4563	3.4076	0.4460	1.9980
Deng [35]	$(\alpha, k) = (4, 0.5)$	(0,0,1,1,1,1,1)	2.1772	1.6269	3.7925	0.5352	2.1158

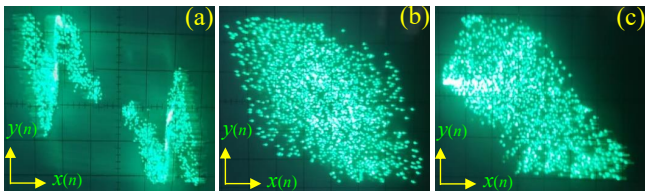

Fig. 12: Experimental results generated by the FPGA-based DDMRNN hardware circuit for different w_{11} values. (a) x-y chaotic attractor with $w_{11} = -10$. (b) x-y chaotic attractor with $w_{11} = 1$. (c) x-y chaotic attractor with $w_{11} = 2.5$.

TABLE III: FPGA RESOURCE UTILIZATION OF THE DESIGNED SYSTEM

Resource	Utilization	Available	Utilization %
LUT	2349	53200	4.42
FF	1563	106400	1.47
DSP	32	220	14.55
IO	34	125	27.20

$$\theta_i = \begin{cases} \arctanh(2^{-i}), \text{if } \mu = -1 \\ 2^{-i}, \text{if } \mu = 0 \\ \arctan(2^{-i}), \text{if } \mu = 1 \end{cases} \tag{7}$$

where n denotes the number of iterations, and k_n represents the scale factor. $\sigma_i = \text{sign}(U_i)$ indicates the direction of the i-th rotation, and θ_i is the angle value of the i-th rotation. When computing the sine function, μ is set to 1; whereas for the hyperbolic tangent function, μ is set to -1. Through successive pseudo-rotations, the actual angle value gradually converges toward the target angle θ. Ultimately, the output results are $\sin(\theta) \approx V_{n+1}$ and $\tanh(\theta) \approx V_{n+1}/U_{n+1}$.

Moreover, after completing synthesis and implementation in the Vivado environment, the FPGA resource utilization of the designed system is listed in Table III. The overall resource utilization of the system is 47.64%, which falls within a reasonable and controllable range.

During the experimental process, we verify the DDMRNN system on hardware using the following specific parameter configuration: coupling strength $k = 1$, delay length $D = 3$, and initial conditions set to $(x(0), y(0), z(0), w(0), w1(0), w2(0), w3(0)) = (0.1, 0.1, 0.1, 0, 0, 0, 0)$. Fig. 12 presents the hardware experimental results under different w_{11} values. Comparative analysis demonstrates that the chaotic attractors observed on the oscilloscope exhibit high consistency with the numerical simulation results shown in Figs. 5(a), (g), and (i). This finding validates the correctness and feasibility of the FPGA-based DDMRNN hardware circuit design.

B. Application in PRNG

The randomness quality of sequences generated by chaotic systems serves as a fundamental metric for evaluating their engineering applicability, which is particularly crucial for chaotic encryption applications [37], [38]. As shown in Table II, the performance assessment results indicate that DDMRNN exhibits good random characteristics. To rigorously validate the system's suitability for cryptographic applications, this study constructs a PRNG based on DDMRNN, employing the rigorous test suite TestU01 and the SP800-22 test standard issued by the National Institute of Standards and Technology (NIST) for comprehensive evaluation of the output sequences. The pseudorandom sequence Pn is produced through the following quantization process:

$$P_n = \lfloor z_n \times M \rfloor \bmod N \tag{8}$$

where $z_n = \{z_1, z_2, \cdots, z_n\}$ represents the chaotic sequence generated by DDMRNN. $\lfloor \cdot \rfloor$ denotes a downward rounding operation. M and N are defined as 2^{24} and 2^8. This conversion process transforms each value in the z_n sequence into an 8-bit binary sequence.

The NIST SP800-22 test suite comprises 15 core statistical test metrics, enabling comprehensive evaluation of local randomness and global distribution properties in pseudorandom sequences. This evaluation framework primarily adopts the pass rate and the P-value as quantitative criteria. The pass rate reflects the proportion of tested sequences that meet the expected statistical test requirements at a given significance level, while the P-value precisely measures the deviation between the observed statistics and the theoretical expectations for ideal random sequences. This experiment employs 128 sets of binary sequences with a length of 10^6 bits as test samples, and the reference thresholds for pass rate and P-value are set at 0.9606 and 0.0001. The parameters and initial values of DDMRNN remain consistent with those specified in Table II.

TABLE IV: NIST RESULTS FOR PSEUDORANDOM NUMBERS GENERATED BY DDMRNN WITH DIFFERENT DELAY LENGTHS

No.	Sub-tests	$D=3$		$D=2$		$D=1$	
		Pass rate	P-value$_T$	Pass rate	P-value$_T$	Pass rate	P-value$_T$
01	Frequency	0.9844	0.1783	0.9922	0.1783	0.9922	0.5174
02	Block Frequency	0.9844	0.1481	1.0000	0.8755	0.9844	0.9114
03	Cum. Sums*(F)	0.9766	0.0542	0.9922	0.0514	1.0000	0.9573
	Cum. Sums*(R)	0.9766	0.1284	0.9922	0.6025	0.9922	0.1783
04	Runs	0.9844	0.4373	0.9844	0.8881	1.0000	0.1413
05	Longest Runs	1.0000	0.2536	0.9844	0.6025	0.9844	0.6025
06	Rank	0.9922	0.2430	0.9844	0.4528	0.9922	0.0669
07	FFT	0.9844	0.7887	0.9922	0.6198	0.9922	0.2645
08	Non-Ovla. Temp.*	0.9895	0.4520	0.9896	0.4356	0.9894	0.4190
09	Ovla. Temp.	0.9922	0.1952	0.9844	0.3505	0.9844	0.5341
10	Universal	0.9844	0.7565	1.0000	0.2993	0.9844	0.2133
11	Appr. Entropy	0.9922	0.6890	0.9844	0.9001	1.0000	0.7061
12	Ran. Exc.*	0.9873	0.3498	0.9868	0.3989	0.9838	0.2826
13	Ran. Exc. Var.*	0.9923	0.2838	0.9889	0.3687	0.9913	0.2482
14	Serial(1st)	0.9844	0.2536	0.9844	0.5174	1.0000	0.9114
	Serial(2nd)	0.9844	0.3925	0.9922	0.3115	0.9922	0.1703
15	Linear complexity	0.9844	0.9573	1.0000	0.3505	0.9844	0.7399
	Success No.	15/15	15/15	15/15	15/15	15/15	15/15

Note: *The average result of multiple subtests is reported.

Detailed test results are summarized in Table IV. The analysis demonstrates that the pass rates and P-values of three test groups are significantly higher than 0.9606 and 0.0001 under different delay lengths D, indicating that DDMRNN possesses excellent randomness properties and is capable of generating high-quality pseudorandom numbers. Notably, when the delay length $D=0$, the pseudorandom sequences generated by the system fail to meet the NIST SP800-22 test standards (the corresponding test data are omitted due to noncompliance).

The TestU01 test suite is a systematic, comprehensive, and rigorous statistical testing tool for random number generators, with superior testing capabilities compared to other commonly used test sets. This suite contains multiple test batteries, each integrating various statistical testing methods. Every test sets the valid P-value range at [0.001, 0.999], and if the P-value of the evaluated sequence falls within this interval, it is considered to have passed the test. In this experiment, we chose five battery sets from TestU01—Rabbit, Alphabit, BlockAlphabit, SmallCrush, and Crush—to test the pseudorandom sequences generated by the system, and the results are summarized in Table V. It can be observed that all three experimental groups with different delay lengths D successfully passed all tests. Notably, when $D=0$, the pseudorandom numbers produced by the system failed to pass the TestU01 tests. Therefore, experimental results from the NIST and TestU01 testing suites demonstrate that the DDMRNN exhibits excellent randomness performance and confirm the crucial role of memristor delay effects in enhancing the dynamical complexity of DDMRNN.

TABLE V: TESTU01 RESULTS FOR PSEUDORANDOM NUMBERS GENERATED BY DDMRNN WITH DIFFERENT DELAY LENGTHS

Batteries	Length of PRNs	$D=3$	$D=2$	$D=1$
Rabbit	128 GB	40/40	40/40	40/40
Alphabit	128 GB	17/17	17/17	17/17
BlockAlphabit	128 GB	102/102	102/102	102/102
SmallCrush	6 GB	15/15	15/15	15/15
Crush	1 TB	144/144	144/144	144/144

V. CONCLUSION

This study proposes a novel discrete memristor model with delay effects and integrates it into a ring HNN to construct a DDMRNN. Through systematic theoretical analysis, we examined the fixed points and stability of the system, discovering the existence of infinitely many unstable points. Further research demonstrates that memristor delay length significantly influences the system's dynamical behavior. In-depth analysis based on LE spectra and bifurcation diagrams reveals that as the delay length increases, the system exhibits progressively more complex nonlinear dynamical characteristics. It is noteworthy that variations in the synapse weight w_{11} can trigger significant dynamical evolution phenomena. This parameter not only induces the generation of diverse attractors but also leads to the emergence of transient chaos and synapse weight-dependent offset-boosting phenomena. More interest-

ingly, multiple types of homogeneous and heterogeneous chaotic attractors coexist under different initial conditions, displaying rich multistability properties. To validate the feasibility of the theoretical model, we designed and implemented a DDMRNN hardware circuit based on an FPGA platform. The experimental results are in high agreement with numerical simulations. Furthermore, we apply the DDMRNN system to PRNG, where the generated random sequences successfully pass the NIST and TestU01 test suites, verifying the system's excellent pseudorandom properties. Future research will focus on two key directions: first, investigating the underlying mechanisms through which discrete memristors with extended delay effects influence neural network dynamics; second, exploring the potential applications of DDMRNN in practical security domains such as image encryption, voice encryption, and secure communication systems.

REFERENCES

[1] P. Baldi and A. F. Atiya, "How delays affect neural dynamics and learning," *IEEE Transactions on Neural Networks*, vol. 5, no. 4, pp. 612–621, 1994.

[2] J.-W. Lin and D. S. Faber, "Modulation of synaptic delay during synaptic plasticity," *Trends in neurosciences*, vol. 25, no. 9, pp. 449–455, 2002.

[3] M. Uzuntarla, M. Ozer, U. Ileri, A. Calim, and J. Torres, "Effects of dynamic synapses on noise-delayed response latency of a single neuron," *Physical Review E*, vol. 92, no. 6, p. 062710, 2015.

[4] R. J. Duro and J. S. Reyes, "Discrete-time backpropagation for training synaptic delay-based artificial neural networks," *IEEE Transactions on Neural Networks*, vol. 10, no. 4, pp. 779–789, 1999.

[5] Q. Yu, J. Gao, J. Wei, J. Li, K. C. Tan, and T. Huang, "Improving multispike learning with plastic synaptic delays," *IEEE Transactions on Neural Networks and Learning Systems*, vol. 34, no. 12, pp. 10 254–10 265, 2022.

[6] C. Liu, J. Wang, H. Yu, B. Deng, X. Wei, J. Sun, and Y. Chen, "The effects of time delay on the synchronization transitions in a modular neuronal network with hybrid synapses," *Chaos, Solitons & Fractals*, vol. 47, pp. 54–65, 2013.

[7] M. Hashemi, A. Valizadeh, and Y. Azizi, "Effect of duration of synaptic activity on spike rate of a Hodgkin-Huxley neuron with delayed feedback," *Physical Review E—Statistical, Nonlinear, and Soft Matter Physics*, vol. 85, no. 2, p. 021917, 2012.

[8] I. Franović and V. Miljković, "The effects of synaptic time delay on motifs of chemically coupled Rulkov model neurons," *Communications in Nonlinear Science and Numerical Simulation*, vol. 16, no. 2, pp. 623–633, 2011.

[9] S. Jain, S. Li, H. Zheng, L. Li, X. Fong, and K.-W. Ang, "Heterogeneous integration of 2D memristor arrays and silicon selectors for compute-in-memory hardware in convolutional neural networks," *Nature Communications*, vol. 16, no. 1, p. 2719, 2025.

[10] B. Xu, X. Luo, Y. Wang, L. Bai, K. Chen, and J. Zhao, "A 4D trigonometric-based memristor hyperchaotic map to ultra-fast PRNG," *IEEE Transactions on Industrial Informatics*, vol. 20, no. 6, pp. 8673–8683, 2024.

[11] Q. Deng, C. Wang, Y. Sun, and G. Yang, "Discrete memristive conservative chaotic map: dynamics, hardware implementation, and application in secure communication," *IEEE Transactions on Cybernetics*, 2025.

[12] R. P. Nelapati *et al.*, "Enhancing digital circuit functionality with a hybrid CMOS-memristor non-volatile D latch: efficiency, reliability, and application," *Engineering Research Express*, vol. 7, no. 1, p. 015363, 2025.

[13] Z. Deng, C. Wang, H. Lin, Q. Deng, and Y. Sun, "Memristor-based attention network for online real-time object tracking," *IEEE Transactions on Computer-Aided Design of Integrated Circuits and Systems*, 2024.

[14] Q. Deng, C. Wang, Y. Sun, X. Cong, H. Lin, and Z. Deng, "Memristor-based brain emotional learning neural network with attention mechanism and its application," *IEEE Transactions on Computer-Aided Design of Integrated Circuits and Systems*, 2025.

[15] W. Yao, K. Gao, Y. Wang, H. Lin, H. Wu, C. Xu, and X. Zhang, "Generalization and differentiation of affective associative memory circuit based on memristive neural network with emotion transfer," *Neural Networks*, vol. 188, p. 107502, 2025.

[16] L. Zhou, J. Han, Z. Zhao, Q. Zhu, and T. Huang, "Global polynomial synchronization of proportional delay memristive competitive neural networks with uncertain parameters for image encryption," *IEEE Transactions on Systems, Man, and Cybernetics: Systems*, 2025.

[17] F. Yu, Y. Wu, X. Wang, T. He, S. Zhang, and J. Jin, "New discrete memristive hyperchaotic map: modeling, dynamic analysis, and application in image encryption," *Frontiers in Physics*, vol. 13, p. 1617964, 2025.

[18] H. Bao, R. Wang, H. Tang, M. Chen, and B. Bao, "Discrete memristive Hopfield neural network with multi-stripe/wave hyperchaos," *IEEE Internet of Things Journal*, 2025.

[19] Q. Wang, Z. Tian, X. Wu, K. Li, H. Sang, and X. Yu, "A 5D super-extreme-multistability hyperchaotic map based on parallel-cascaded memristors," *Chaos, Solitons & Fractals*, vol. 187, p. 115452, 2024.

[20] D. Luo, C. Wang, Q. Deng, and G. Yang, "Discrete memristive hyperchaotic maps with high Lyapunov exponents," *Nonlinear Dynamics*, vol. 113, pp. 28 381–28 395, 2025.

[21] Q. Lai, C. Zhu, X.-W. Zhao, X. Sun, and J. Hua, "A unified framework for generating 4D discrete memristive hyperchaotic maps with complex dynamics and application to encryption," *IEEE Internet of Things Journal*, 2025.

[22] J. Ma and J. Tang, "A review for dynamics in neuron and neuronal network," *Nonlinear Dynamics*, vol. 89, no. 3, pp. 1569–1578, 2017.

[23] J. J. Hopfield, "Neural networks and physical systems with emergent collective computational abilities." *Proceedings of the national academy of sciences*, vol. 79, no. 8, pp. 2554–2558, 1982.

[24] X. Peng, C. Li, Y. Zeng, and C.-L. Li, "Adjusting dynamics of Hopfield neural network via time-variant stimulus," *IEEE Transactions on Circuits and Systems I: Regular Papers*, vol. 71, no. 7, pp. 3242–3255, 2024.

[25] C. Wang, Y. Li, G. Yang, and Q. Deng, "A review of fractional-order chaotic systems of memristive neural networks." *Mathematics (2227-7390)*, vol. 13, no. 10, 2025.

[26] H. Lin, X. Deng, F. Yu, and Y. Sun, "Grid multibutterfly memristive neural network with three memristive systems: Modeling, dynamic analysis, and application in police IoT," *IEEE Internet of Things Journal*, vol. 11, no. 18, pp. 29 878–29 889, 2024.

[27] F. Yu, C. Wu, Y. Lin, S. He, W. Yao, S. Cai, and J. Jin, "Dynamic analysis and hardware implementation of multi-scroll Hopfield neural networks with three different memristor synapses," *Nonlinear Dynamics*, vol. 112, no. 14, pp. 12 393–12 409, 2024.

[28] D. Luo, C. Wang, J. Liang, and Q. Deng, "Memristor coupled fractional-order hopfield neural network composed by heterogeneous neurons and its fpga implementation," *Nonlinear Dynamics*, pp. 1–16, 2025.

[29] S. Zhang, Y. Li, X. Wang, and Z. Zeng, "Initial offset-boosted coexisting hidden chaos and firing multistability in memristive ring neural network with hardware implementation," *IEEE Transactions on Industrial Electronics*, 2024.

[30] S. Zhang, Y. Li, D. Lu, X. Gao, C. Li, and G. Chen, "A novel memristor regulation method for chaos enhancement in unidirectional ring neural networks," *IEEE Transactions on Circuits and Systems I: Regular Papers*, 2025.

[31] B. Bao, H. Tang, H. Bao, Z. Hua, Q. Xu, and M. Chen, "Simplified discrete two-neuron Hopfield neural network and FPGA implementation," *IEEE Transactions on Industrial Electronics*, 2024.

[32] H. Bao, J. Fan, Z. Hua, Q. Xu, and B. Bao, "Discrete memristive Hopfield neural network and application in memristor-state-based encryption," *IEEE Internet of Things Journal*, 2025.

[33] W. Liu, K. Sun, H. Wang, and B. Li, "Delayed feedback chaotification model and its hardware implementation," *IEEE Transactions on Industrial Electronics*, vol. 71, no. 10, pp. 13 002–13 011, 2024.

[34] Q. Deng, C. Wang, Y. Sun, and G. Yang, "Delay difference feedback memristive map: Dynamics, hardware implementation, and application in path planning," *IEEE Transactions on Circuits and Systems I: Regular Papers*, 2025.

[35] Q. Deng, C. Wang, G. Yang, and D. Luo, "Discrete memristive delay feedback Rulkov neuron model: Chaotic dynamics, hardware implementation and application in secure communication," *IEEE Internet of Things Journal*, 2025.

[36] K. Pyragas, "Continuous control of chaos by self-controlling feedback," *Physics letters A*, vol. 170, no. 6, pp. 421–428, 1992.

[37] S. Gao, R. Wu, H. H.-C. Iu, U. Erkan, Y. Cao, Q. Li, A. Toktas, and J. Mou, "Chaos-based video encryption techniques: A review," *Computer Science Review*, vol. 58, p. 100816, 2025.

[38] S. Gao, Z. Zhang, Q. Li, S. Ding, H. H.-C. Iu, Y. Cao, X. Xu, C. Wang, and J. Mou, "Encrypt a story: A video segment encryption method based on the discrete sinusoidal memristive rulkov neuron," *IEEE Transactions on Dependable and Secure Computing*, 2025.

Gang Yang received the B.S. degree in communications engineering and the M.S. degree in artificial intelligence form the Jiangxi University of science and technology, Ganzhou, China, in 2020 and 2023, respectively. He is currently pursuing the Ph.D degree with the college of computer science and electronic engineering, Hunan University, Changsha, China.

His current research interests include chaotic systems and circuits, memristor neural networks, and memristor systems and circuits.

Chunhua Wang received the M.S. degree in microphysics from Zhengzhou University, Zhengzhou, China, in 1994, and the Ph.D. degree in microelectronics and solid-state electronics from Beijing University of Technology, Beijing, China, in 2003.

He is currently a Professor with the College of Computer Science and Electronic Engineering, Hunan University, Changsha, China, where he is also a Doctor Tutor and the Director of the Advanced Communication Technology Key Laboratory. He has presided over more than eight national and provincial projects and authored or co-authored more than 200 articles retrieved by SCI, among which 20 articles were highly cited. His research interests include chaotic circuits, memristor circuits, chaotic encryption, neural networks based on memristor, complex networks, and current-mode circuits.

Dr. Wang is the Director of the Chaos and Nonlinear Circuit Professional Committee of the Circuit and System Branch of the China Electronic Society.

Yichuang Sun (Senior Member, IEEE) received the B.Sc. and M.Sc. degrees from Dalian Maritime University, Dalian, China, in 1982 and 1985, respectively, and the Ph.D. degree from the University of York, York, U.K., in 1996, all in communications and electronics engineering.

Dr. Sun is currently Professor of Communications and Electronics, Head of Communications and Intelligent Systems Research Group, and Head of Electronic, Communication and Electrical Engineering Division in the School of Engineering and Computer Science of the University of Hertfordshire, UK. He has published over 420 papers and contributed 10 chapters in edited books. He has also published four text and research books: Continuous-Time Active Filter Design (CRC Press, USA, 1999), Design of High Frequency Integrated Analogue Filters (IEE Press, UK, 2002), Wireless Communication Circuits and Systems (IET Press, 2004), and Test and Diagnosis of Analogue, Mixed-signal and RF Integrated Circuits - the Systems on Chip Approach (IET Press, 2008). His research interests are in the areas of wireless and mobile communications, RF and analogue circuits, memristor circuits and systems, and machine learning and neuromorphic computing.

Quanli Deng received the B.S. degree in microelectronics from the School of Physics and Optoelectronics, Xiangtan University, Xiangtan, China, in 2016, and the M.S. degree in information and communication engineering and the Ph.D. degree in computer science and technology from the College of Computer Science and Electronic Engineering, Hunan University, Changsha, China, in 2020 and 2024, respectively.

He is currently a Post-Doctoral Research Fellow with the College of Computer Science and Electronic Engineering, Hunan University. His research interests include modeling and analysis of neural systems, fundamental theory of nonlinear systems and circuits, and analog implementation of neuromorphic systems.